Extracellular fluid viscosity enhances liver cancer cell mechanosensing and migration

Jordi Gonzalez-Molina*[1], Xiaoli Zhang[2], Michela Borghesan[1], Joana Mendonça da Silva, Maooz Awan[1], Barry Fuller[3], Núria Gavara[2], and Clare Selden[1]

[1] UCL Institute for Liver and Digestive Health, UCL - Royal Free Hospital Campus, UCL Medical School, NW3 2PF, London, UK.

[2] School of Engineering and Materials Science, Queen Mary University of London, Mile End Road, E1 4NS, London, UK.

[3] Department of Surgery, Royal Free Hospital, UCL Medical School, NW3 2QG, London, UK.

*Correspondence to: j.molina@ucl.ac.uk

Declarations of interest: none

Abstract

The extracellular fluid (ECF) is a crowded environment containing macromolecules that determine its characteristic density, osmotic pressure, and viscosity, which greatly differ between tissues. Precursors and products of degradation of biomaterials enhance ECF crowding and often increase its viscosity. Also, increases in ECF viscosity are related to mucin-producing adenocarcinomas. However, the effect of ECF viscosity on cells remains largely unexplored. Here we show that viscosity-enhancing polymer solutions promote mesenchymal-like cell migration in liver cancer cell lines. Also, we demonstrate that viscosity enhances integrin-dependent cell spreading rate and causes actin cytoskeleton re-arrangements leading to larger cell area, nuclear flattening, and nuclear translocation of YAP and β-catenin, proteins involved in mechanotransduction. Finally, we describe a relationship between ECF viscosity and substrate stiffness in determining cell area, traction force generation and mechanotransduction, effects that are actin-dependent only on $\leq$ 40 kPa substrates. These findings reveal that enhancing ECF viscosity can induce major biological responses including cell migration and substrate mechanosensing.

1. Introduction

The mechanical characteristics of the extracellular matrix (ECM) largely depend on its composition of elastic fibres, fibrillar collagens, and proteoglycans [1]. These findings have led to the design of biomaterials with well-defined physical characteristics including remodelling properties, visco-elasticity, fibre architecture, and crosslinking density, which at the same time have contributed to the understanding of the cellular microenvironment [2]. Likewise, the physical attributes of the extracellular fluid (ECF) in different biological fluids present characteristic osmotic pressure, hydrostatic pressure, and viscosity that induce mechanical stimuli sensed by cells. These physical features of the extracellular milieu greatly affect cell behaviour of normal and cancer cells [3]. Furthermore, the osmotic and hydrostatic interstitial fluid pressures are often elevated in solid tumours [4]. Osmotic pressure causes a rapid change in cell volume leading to membrane mechanical adaptations [5]. However, models of osmotic pressure given by glycosaminoglycans in tumours predict negligible contributions of osmotic pressure compared to interstitial hydrostatic pressure [6]. Interstitial fluid pressure has been found to regulate the collective migration of tumour cells *in vitro* and its reduction decreases cell proliferation *in vivo* [7, 8]. Additionally, ECF viscosity enhances epithelial ciliary activity and, as a direct contributor to shear stress in flowing fluids, causes endothelial cell alignment and influences vascular development and cancer cell migration [9-13].

Viscosity of the ECF may be altered by the introduction of soluble polymers that can be precursors or products of the degradation of solid biomaterials. Also, naturally produced molecules such as mucins, expressed in various epithelial mucosal cells of the respiratory, digestive, and urogenital tracts, as well as in organs such as liver, pancreas, gallbladder, kidneys, and salivary glands, are strong viscosity enhancers [14]. Viscosity of mucus greatly varies with mucin concentration, pH, ionic strength, temperature, and shear rate. At low shear rates, viscosity values range from 1,000 cP in airway mucus to 6,000 cP in gastric mucus [15]. Mucins are highly expressed in mucin-producing adenocarcinomas, promote tumour growth and survival, and are a marker of poor prognosis [16]. The viscosity of the interstitial fluid is

typically < 2 cP [17], but the presence of macromolecules can dramatically increase its viscosity. Even though extracellular fluids normally have a considerably large content of macromolecules [18], the impact of macromolecular crowding and viscosity caused by these macromolecules on cell behaviour remains largely unexplored. Moreover, the effect of viscosity, which has been demonstrated in isolated biochemical reactions, is poorly understood at the cellular level [19-21].

Various molecules at the interface between the cell surface and the extracellular environment have been involved in mechanical sensing. Amongst these, integrins are the most widely studied. Integrins are transmembrane proteins that bind to ECM ligands and are responsible for transmitting and applying force to the ECM [22]. The force transmission process can be explained by the molecular clutch model of mechanotransduction [23]. This model explains rigidity sensing considering the differences in integrin-ECM bond lifetime and force loading rates in soft and stiff substrates determining force transmission to the intracellular protein talin, which leads to adhesion reinforcement and mechanotransduction pathway activation [24]. Interestingly, reducing the diffusion of integrin ligands by increasing the surface viscosity of purely viscous cellular substrates has been shown to enhance force loading rate, activating mechanotransduction pathways [25]. Moreover, pulling forces applied by integrin-based focal adhesions and the activation of the focal adhesion kinase (FAK)/phosphopaxillin/vinculin pathway explain the process by which cells migrate towards areas of high ECM rigidity [26].

Based on these studies, we hypothesised a role for static ECF viscosity on cell migration and substrate mechanotransduction. To address this hypothesis, we evaluated the effect of various soluble polymers and mucin on the migration of liver cancer cell lines with epithelial and mesenchymal phenotypes. To explore the effect of cell-substrate adhesion dynamics we monitored cells over time using integrin-dependent and -independent substrates. Also, we evaluated the activation of mechanotransduction pathways upon exposure to high ECF viscosity. Finally, we studied the relationship between substrate stiffness and ECF viscosity on determining cell behaviour. Our data indicate that polymer-enhanced viscosity induces

mesenchymal cell migration and affects both cell-substrate adhesion dynamics and mechanical sensing leading to a mesenchymal-like behaviour in liver epithelial cancer cell lines.

2. Materials & methods

2.1. Viscous media preparation

High viscosity, G-rich, sodium alginate (FMC Biopolymer) and low viscosity, G-rich, Na-alginate (Sigma), and polyethylene glycol (PEG M_w 300; 6,000; 20,000; and 1,000,000) (Sigma) were prepared as 2% solutions in 0.15 M NaCl 2% HEPES (Gibco) adjusted at pH 7.4. Dextran from *Leuconostoc* spp. (M_w 450,000 – 650,000, Sigma) and Mucin type II from porcine stomach (Sigma) were prepared as 20% solutions in 0.15 M NaCl 2% HEPES adjusted at pH 7.4. For 0% polymer controls, 0.15 M NaCl 2% HEPES pH 7.4 solutions were used. 50% complete cell culture medium and 50% solutions or control were mixed to obtain 1% solutions of Na-alginate and PEG, and 10% solution of mucin and dextran and subsequently filter-sterilised. To control PEG-enhanced osmotic pressure, 1% PEG 20,000 and 1% PEG 1,000,000 solutions were adjusted with PEG 6,000 to contribute a total of 0.5 mOsm to the final solutions. Calcium alginate hydrogel was formed by crosslinking high viscosity Na-alginate with 200 mM $CaCl_2$ in 0.15 M NaCl at pH 7.4 for 2 min, and subsequently washed with Hanks' Balanced Salt Solution (HBSS, Gibco) to remove excess calcium. Viscosities of final solutions were measured with a cone/plate viscometer (Brookfield DV-II+Pro) with a CP(E)-41 spindle at shear rates ranging from 2 to 300 s^{-1} at a controlled temperature of 37 °C. All viscosity values in the main text correspond to values at 100 s^{-1} shear rate.

2.2. Cell culture

HepG2, SKHEP1, and Huh7 (ATCC) cells were cultured in Minimum Essential Medium with alpha modification (MEMalpha, GE Healthcare) supplemented with 10% Fetal Calf Serum

(FCS, Hyclone), and 100 IU/ml penicillin and 0.1 mg/ml streptomycin. C3A and PLC/PRF/5 cells (ATCC) were maintained in Dulbecco's Modified Eagles Medium (DMEM, Gibco) supplemented with 10% FCS and 100 IU/ml penicillin and 0.1 mg/ml streptomycin. SNU475 cells (ATCC) were cultured in Roswell Park Memorial Institute 1640 (RPMI-1640, Gibco) supplemented with 10% FCS and 100 IU/ml penicillin and 0.1 mg/ml streptomycin.

2.3.   Wound healing assay

Cells were seeded on 6-well plates. When confluency was reached, the monolayer was scratched with a 20 μl pipette tip. Non-attached cells were removed by washing with HBSS twice, and media was changed to 0% control or 1% Na-alginate (FMC Biopolymer). For comparison between different alginates low viscosity Na-alginate (Sigma) was also used. Also, 1% PEG 20,000 and 1% PEG 1,000,000 were used for this assay for comparison and to avoid the effect of alginate crosslinking by the calcium present in the culture medium. Images were taken at 0 h and at different time points for each cell line. Each well was imaged at 6-10 fixed positions. For chemical induction of epithelial-to-mesenchymal transitition (EMT), Huh7 cells were cultured in complete medium with 20 μg/ml hepatocyte growth factor (HGF, Peprotech) 24 h prior to and during each experiment. Images were acquired with a Nikon TE200 microscope with a Nikon DS-Fi1c camera (with a 0.67x adapter), DS-U2 PC control unit and NIS Elements software. The TScratch software was used to calculate the percentage of wound closure as previously described [27].

2.4.   Cell number

To determine the total cell number, 5 x 10^4 cells per well were seeded in 12-well plates. After a 4-day treatment, cells were washed with PBS and detached from the wells with TrypLE Select (Gibco). Total nuclei were counted by automated cell nuclei quantitation (Nucleocounter, Sartorius-Stedim).

2.5.   Gene expression analysis.

HepG2 cells on tissue culture plates at a ~15 % confluency were treated with control medium (0% Na-alginate or 1% PEG 20,000) or viscous media (1% High viscosity Na-alginate (FMC Biopolymer) or 1% PEG 1,000,000 (Sigma)) for 48 h. Total RNA was extracted by the TRIzol method (Thermofisher) following the manufacturer's protocol. Reverse transcription reaction and polymerase chain reaction (PCR) was conducted with 250 ng of total RNA per sample with the Luna Universal one-step RT-qPCR kit (New England Biolabs). Specific primers were used and relative gene expression was quantified using the $2^{-\Delta\Delta Ct}$ method and normalized to HPRT1 expression (and validated with GAPDH) and then compared to control cells. Primer sequences:

GAPDH (5'-GACCCCTTCATTGACCTCAAC-3', 5'- CTTCTCCATGGTGGTGAAGA-3'),
HPRT1 (5'- AGACTTTGCTTTCCTTGGTCAG-3', 5'- TCAAGGGCATATCCTACAACAA-3'),
CDH1 (5'- TGCCCAGAAAATGAAAAAGG-3', 5'- GTGTATGTGGCAATGCGTTC-3'),
CDH2 (5'- ACAGTGGCCACCTACAAAGG-3', 5'- CCGAGATGGGGTTGATAATG-3'),
FN1 (5'- CAGTGGGAGACCTCGAGAAG-3', 5'- TCCCTCGGAACATCAGAAAC-3'),
CTGF (5'- ACCGACTGGAAGACACGTTTG-3', 5'- CCAGGTCAGCTTCGCAAGG-3'),
AREG (5'- CTGGGAAGCGTGAACCATTTT-3', 5'- TCTGAGTAGTCATAGTCGGCTC -3'),
BIRC5 (5'- AGGACCACCGCATCTCTACAT-3', 5'- AAGTCTGGCTCGTTCTCAGTG -3'),
GLUL (5'- GTGAAGACTTTGGAGTGATAG-3', 5'- GATGTACTTCAGACCATTCTC-3'),
CCND1 (5'- GCCTCTAAGATGAAGGAGAC-3', 5'- CCATTTGCAGCAGCTC-3'),
AXIN2 (5'- AAAGAGAGGAGGTTCAGATG-3', 5'- CTGAGTCTGGGAATTTTTCTTC-3').

2.6. Immunostaining

Medium was removed and cells were immediately fixed with cold 4% paraformaldehyde in PBS for 15 min, permeabilised with 0.3% Triton X-100 for 10 min for intracellular/nuclear protein staining or with 0.1% Triton X-100 for 5 minutes for actin cytoskeleton and paxillin staining and blocked for 1 h with 3% Bovine Serum Albumin (BSA, Sigma). Samples were incubated overnight at 4 °C with primary antibodies YAP (1:200, Cat. Num. sc-101199, Scbt), β-catenin (1:200, Cat. Num. sc-101199, Scbt), twist1 (1:200, Cat. Num. T6451, Sigma), paxillin (1:100, Cat. Num. ab32084 Abcam). Secondary antibodies anti-Rabbit IgG-PE (Cat. Num. sc-

3739, Scbt) or anti-mouse IgG-488 (Cat. Num. A-11059, Thermofisher) were subsequently incubated (1:500) for 1 h at room temperature. Hoechst 33342 (Sigma) and phalloidin-488 (1:1000; Cat. Num. sc-363791, Scbt) were used to stain nuclei and actin cytoskeleton, respectively. Images were acquired with an INCell Analyser 2200 automated microscope (GE Healthcare Life Sciences) with a CMOS camera.

2.7. Inhibition studies

For pharmacological inhibition, 2 μg/ml Cytochalasin B (Sigma), 1 μM Nocodazole (Sigma), 20 μM blebbistatin (Medchem), 20 μM Y27632 (Medchem), and 20 μM PF-573228 (Medchem) were used with a 1 h pre-treatment to ensure inhibition and subsequent treatment.

2.8. Cell spreading assay

13 mm diameter glasses were functionalised by silanizing with (3-aminopropyl)trimethoxysilane (APTMS, Sigma) and subsequently treated with 0.5% glutaraldehyde, washed extensively with deionised water and incubated overnight at 4°C with 10 μg/ml of human fibronectin (Roche), reconstituted basement membrane from Engelbreth-Holm-Swarm murine sarcoma (Sigma), or poly-L-lysine (Sigma). Prior to cell seeding, glasses were washed twice with PBS (Gibco) and twice with serum-free cell culture medium. A total of 2.5 x 10^4 cells/well in serum-free medium were seeded. Cells were monitored until they were attached but not spread, maintaining a round morphology. Unattached cells were removed by washing with HBSS three times. In RGD peptide-treated cells, 10 μM RGD peptide (MedChem) was used during treatment. Cells were exposed to different conditions at 37 °C and images were taken at different time intervals according to each cell type. Images were acquired with a Nikon TE200 microscope with a Nikon DS-Fi1c camera (with a 0.67x adapter), DS-U2 PC control unit and NIS Elements software. Images of live cells were analysed considering spread cells those with at least twice the average of non-spread size and/or loss of circular morphology using ImageJ.

2.9. Polyacrylamide gel preparation

To prepare polyacrylamide gels, glass slides (13 or 22 mm diameter) were silanized with (3-aminopropyl)trimethoxysilane (APTMS, Sigma) and subsequently treated with 0.5% glutaraldehyde. Mixtures of deionised water, acrylamide monomers, crosslinker *N,N* methylene-bis-acrylamide, ammonium persulphate and *N,N,N',N'*-tetramethylethylenediamine (TEMED) were prepared at different concentrations to achieve 1, 4.5, 8.5, 10, 20, 40, or 115 kPa gels according to previously determined formulations [28, 29]. For Traction Force experiments 4 μl of 0.2 μm fluorescent beads (FluoSpheres, Molecular probes) were added to 0.5 ml of non-polymerised mixtures. To allow cell adhesion, gels were treated with *N*-sulphosuccinimidyl-6-(4′-azido-2′-nitrophenylamino) hexanoate (sulpho-SANPAH, Sigma), activated with ultraviolet light. Activated gels were then incubated with 50 μg/ml human fibronectin (Roche) overnight at 4 °C and UV-sterilised prior to cell seeding.

2.10. Cell image analyses

Inter-nuclear distance for cell scattering experiments was measured after 24 h treatments on fixed, Hoechst 33342-stained cells with the NIS-Elements Microscope Imaging software (Nikon) measuring the distance between the nucleus periphery and that of their nearest neighbour nucleus. Cell area and circularity (4π x area/perimeter^2) measurements were made with the NIS-Elements Microscope Imaging software from phase contrast images of well delimited cells. For YAP and β-catenin, cytoplasmic and nuclear localisation, Hoechst 33342-stained nuclei images were used to determine nuclei location. Average fluorescent intensity of defined regions of interest in the nucleus and cytoplasm/membrane was measured with the NIS-Elements Microscope Imaging software and nucleus:cytoplasm ratio of >1.5 was used to define nuclear localisation of the protein.

2.11. Single cell nuclear flattening and confocal imaging for protein localisation

HepG2 cells were seeded at low density on chambered coverglass Lab-Tek II (Nunc) and let to adhere overnight at 37 °C. Cells were treated with 1% PEG 20,000 or 1% PEG 1,000,000 with 2 μg/ml cytochalasin B (Sigma) or equivalent volume of DMSO (Sigma) for 6 h or 24 h at

37 °C and 5% CO_2 in a humidified incubator. After incubation, cells were fixed and immunostained for YAP, β-catenin, and nuclei. Fluorescence images were taken with a 60X oil immersion objective (NA = 1.4) in a Nikon Eclipse Ti-E inverted microscope. Protein localisation was measured by obtaining average fluorescence intensities of selected regions of interest in the nucleus (defined by Hoechst 33342 staining) and the cytoplasm adjacent to it with the NIS-Elements Microscope Imaging software. To analyse nuclear flattening, 3D reconstructions of nuclei were used and length/height ratio was measured to determine nuclear flattening.

2.12.   Live cell imaging

HepG2 cells were transfected with Actin-GFP with Lipofectamine LTX (ThermoFisher) to visualize F-actin localization within the cells. In order to image single cell dynamics, transfected cells were seeded at low density. After changing medium to 1% PEG 20,000 or 1% PEG 1,000,000 medium, the cellular response was imaged up to 10 h with a frame rate of 5 min. Time-lapse recordings were acquired at 20X magnification using an epifluorescence microscope system housed inside an incubator (Lumascope 720, Etaluma) equipped with a high sensitivity monochrome CMOS camera. The microscope was placed in an incubator to maintain the temperature at 37°C and CO_2 concentration at 5%. Image analysis was performed using customised routines under Matlab (Mathworks).

2.13. Traction force measurements.

1.25×10^4 HepG2 cells or PLC/PRF/5 cells were seeded on 4.5 kPa or 8.5 kPa fibronectin-functionalised polyacrylamide gels, respectively, each containing fluorescent beads, and left to attach overnight. HepG2 cells were treated for 1.5 h and PLC/PRF/5 cells for 3 h with either 1% PEG 20,000 or 1% PEG 1,000,000 before imaging the stressed gels. To obtain images from relaxed gels, cells were lysed by adding 25 μl of 20% (w/v) SDS solution. To compute traction forces exerted by the cells on the gel, the displacement field was first computed using image correlation by comparing the fluorescence images of stressed and relaxed gel. Traction

force field was computed by common constrained Fourier transform traction cytometry (CFTTC) algorithms, using E values of the corresponding gel. Cell area, total cell traction force, and traction stress were calculated.

2.14. Statistical analysis

Statistical analyses were carried out using GraphPad Prism or Microsoft Excel. When two groups were compared, two-tailed Student's t-test was used, and when more groups were compared, analysis of variance (ANOVA) was carried out. For data not meeting normal distribution, equivalent non-parametric tests were applied. Significance was considered at $p < 0.05$. Details of specific tests, repeats, sample numbers, and data and error descriptions are detailed in figure legends.

3. Results

3.1. Na-alginate enhances would healing

To investigate the effect of viscosity of static fluids on cancer cell migration, we used a variety of liver cancer cell lines with mesenchymal and epithelial characteristics and the inert viscosity enhancer sodium alginate (1% Na-alginate; 64.7 cP at 37 °C and a shear rate of 100 s^{-1}). Cell migration assessed by a wound healing assay revealed that Na-alginate promotes wound closing in cells with mesenchymal phenotype (Fig. 1A). Interestingly, the epithelial cell line HepG2 and its derived clone C3A also presented faster wound healing in 1% Na-alginate (Fig. 1B). Based on these results, we used the HepG2 cell line to further study the effects of ECF viscosity. We compared the effect of two different commercially available Na-alginates at 1% w/v (64.7 and 6.5 cP). Both alginate-containing solutions, which are considerably more viscous than the interstitial fluid of most healthy tissues (< 2 CP), presented a significantly faster wound closing than 0% alginate control (~ 1 cP) (Fig. 1C). Likewise, the wound closing of cells exposed to the 64.7 cP solution was significantly faster than cells exposed to the 6.5 cP solution. Moreover, faster wound closing was not explained by an enhanced cell proliferation

rate in 64.7 cP Na-alginate treated cells (Fig. 1D), suggesting that viscous Na-alginate solutions enhance cell migration.

3.2. High extracellular viscosity induces cell scattering and migration in HepG2 cells

We hypothesised that HepG2 cells acquire a mesenchymal phenotype under viscous conditions. A characteristic of epithelial-to-mesenchymal transition (EMT) is the scattering of cells due to increased migration and loss of cell-cell junctions leading to a dissemination of cells from the original cluster [30]. Thus, we examined whether high viscosity caused cell scattering in HepG2 cell clusters. Increasing ECF viscosity with various polymers but not an insoluble form of alginate, Ca-alginate, enhanced the internuclear distance, as observed in cell scattering (Fig. 2A and B). To rule out an effect of osmotic pressure, volume exclusion, and differences in molecular structure, we compared the cell scattering effects produced by polyethylene glycol (PEG) with varying molecular weights but equal concentration (1% (w/v)). Only high viscosity PEG 1,000,000 (40.0 cP) caused an enhanced internuclear distance in HepG2 cells relative to 0% control (Fig. 2C). Also, we compared the scattering effect of 1% PEG 1,000,000 (40.0 cP) and 1% PEG 20,000 (3.2 cP) after equalising the osmolarity of the solutions with PEG 6,000. As expected, the internuclear distance of cells treated with 1% PEG 1,000,000 was significantly larger than 1% PEG 20,000 (Supplementary Fig. S1A). Moreover, 1% PEG 1,000,000 significantly enhanced wound healing in HepG2 cells compared with 1% PEG 20,000 (Supplementary Fig. S1B). Together, these data indicate that high ECF viscosity enhances wound healing due to cell scattering in HepG2 cells.

3.3. High viscosity induces morphological changes without a typical EMT gene expression

Cell scattering observed in EMT is usually accompanied by morphological changes, actin cytoskeleton rearrangements, and loss of cell-cell contacts to facilitate cell migration [30]. A 1% PEG 1,000,000 exposure, but not 1% PEG 20,000, caused disruption of cell-cell junctions and the formation of actin stress fibres and lamellipodia in initially clustered HepG2 cells (Fig.

2D). Furthermore, PEG 1,000,000-treated cells presented an enhanced cell area and reduced circularity (Fig. 2E and F). Similar effects were also observed with other viscosity enhancers (Supplementary Fig. S2A – C). To confirm a direct effect of viscosity on cell migration, we used time-lapse microscopy to track single HepG2 cells, demonstrating an increased cell velocity in viscous PEG 1,000,000-containing medium (Fig. 2G). However, EMT-related gene expression analysis did not show downregulation of epithelial E-cadherin (*CDH1*) or upregulation of mesenchymal N-cadherin (*CDH2)* and fibronectin (*FN1*) markers, indicating that viscosity induces a mesenchymal-like behaviour without a typical EMT phenotype (Fig. 2F – H). Analysis of morphology in other cell lines revealed no variations in cell area, at 24 h treatment, in epithelial PLC/PRF/5 and mesenchymal SK-HEP-1 cells but a significant increase in epithelial Huh7 cells (Supplementary Fig. 2D – F). Also, in PLC/PRF/5 cells actin-rich short protrusions were observed (Supplementary Fig. S2G and H) indicating that other cell lines are also influenced by ECF viscosity. These results demonstrate that static ECF viscosity induces cell migration affecting the organisation of the actin cytoskeleton without a switch from epithelial to mesenchymal gene expression.

3.4. Viscosity-enhanced cell area is actomyosin- and tubulin-independent

We hypothesised that the actin cytoskeleton and focal adhesions are essential to transduce viscosity-induced mechanical signals causing morphological and motile effects as previously reported in the sensing of substrate mechanics [22]. To test this hypothesis, we pharmacologically disrupted the actin cytoskeleton and inhibited Rho-associated protein kinase (ROCK) and myosin II-based contractility and focal adhesion kinase (FAK) and found that FAK activity and the actin cytoskeleton, but not its contractility, are necessary for viscosity-induced enhanced internuclear distance (Fig. 3A). Moreover, inhibition of ROCK caused an enhanced internuclear distance in both low and high viscosity conditions (Supplementary Fig. S2I and Fig. 3A). Strikingly, these inhibitions could not abolish the effect of viscosity on cell area (Fig. 3B and C), but, as expected, actin disruption blocked protrusion and stress fibre formation (Fig. 3D and E). Also, microtubule disruption with nocodazole or combined actin and

tubulin inhibition did not affect cell area in high viscosity-treated cells but enhanced cell circularity (Fig. 3F and G). Thus, viscosity-enhanced cell scattering is actomyosin/FAK-dependent but cell area is actomyosin/FAK-independent.

3.5.   Viscosity enhances integrin-dependent cell spreading

Since viscosity enhances cell area but generally resists the motion of particles within fluids, we investigated the effect of viscosity on cell area dynamics. Time-lapse imaging revealed a steady increase in average cell area in HepG2 cells exposed to 1% PEG 1,000,000 reaching a plateau after 320 min (Fig. 4A). However, analyses of individual cells indicated rapid increases in cell area followed by fast retractions (~ ±100 μm^2/min) (Fig. 4B and C). Based on these observations, we speculated an effect of viscosity on cell-substrate adhesion dynamics. We monitored cell spreading over time and evaluated whether this effect was integrin-dependent by using fibronectin (FN) or poly-L-lysine (PLL) coated glass. Viscous PEG significantly enhanced cell spreading over FN-glass, an effect blocked by the presence of integrin-binding soluble RGD peptides and by PLL-coated surfaces (Fig. 4D – F). These effects were observed in all other cell types investigated, as well as with Na-alginate and dextran, and in cells adhered to reconstituted basement membrane-coated glass (Supplementary Fig. S3). Together, these results indicate, in contrast to other protein – ligand interactions [19], that viscosity facilitates integrin-dependent cell-substrate attachment resulting in enhanced cell spreading.

3.6.   High ECF viscosity causes nuclear translocation of YAP and β-catenin

Given the observed changes in cell morphology and migration induced by viscosity, a mechanical stimulus, we speculated an involvement of mechanotransduction pathways responding to ECF viscosity. We explored potential effects of viscosity on the transcription factors yes-associated protein (YAP), β-catenin, and Twist1, which are involved in migration, EMT, and respond to extracellular mechanical stimuli [31-35]. When exposing HepG2 cells to high viscosity, both β-catenin and YAP translocated from the membrane to the cytoplasm and

nucleus, but Twist1 remained nuclear in both conditions (Fig. 5A). Gene expression analysis of YAP and β-catenin target genes revealed a pronounced upregulation of amphiregulin (*AREG*) but a downregulation of survivin (*BIRC5*) and connective tissue growth factor (*CTGF*) (Fig. 5B and C). Interestingly, upregulation of *AREG* by YAP induces cell migration without EMT in mammary epithelial cells [36] but CTGF and BIRC5 have been linked to EMT [37, 38], suggesting that other factors may be contributing to suppress EMT-related gene expression. Next, we explored the role of actomyosin and FAK in YAP and β-catenin nuclear translocation in HepG2 cells. Only the inhibition of FAK partially reduced nuclear YAP+ cells, but translocation of β-catenin was unaffected (Supplementary Fig. S4A and Fig. 5D and E). Similarly, PLC/PRF/5 cells in high viscosity showed enhanced YAP nuclear localisation which was maintained in actomyosin/FAK pharmacologically inhibited conditions (Supplementary Fig. S4B and C). Moreover, microtubule disruption did not block this translocation in either cell type (Supplementary Fig. S4D and E). Thus, we sought to explore the role of morphology and cell-cell junctions in YAP/β-catenin localisation as these were unchanged upon actomyosin/FAK inhibition. To investigate whether YAP/β-catenin localise in cell-cell junctions as previously described in other epithelial cells [32], we used low-viscosity low-cell density cultures. As expected, both β-catenin and YAP accumulated at the membrane in cell-cell junctions (Supplementary Fig. S5A). Consequently, we investigated the contribution of loss of cell-cell junctions to YAP and β-catenin nuclear translocation. At high ECF viscosity, dense cultures effectively blocked the translocation of YAP and β-catenin (Fig. 6A). Comparable results were obtained with epithelial PLC/PRF/5 cells (Supplementary Fig. S5B). However, a complete loss of cell-cell contacts in low viscosity single cells did not increase nuclear YAP and β-catenin to the levels found in viscosity-treated cells. This effect was independent of actin cytoskeleton integrity at 24 h but not at 6 h of treatment (Fig. 6B and C). Hence, we explored the effect of cell area on YAP and β-catenin nuclear translocation. Cell area in single HepG2 cells presented a positive correlation with nuclear:cytoplasmic ratio of YAP and β-catenin (p < 0.001, Spearman's rank correlation) (Fig. 6D and E). Also, a recent study shows that YAP

nuclear entry is promoted in force-induced nuclear flattening [39]. Therefore, we analysed nuclear flattening in viscosity-treated single cells. Nuclei of cells in viscous ECF appeared to be flatter than in non-viscous ECF, and actin disruption was unable to inhibit nuclear flattening at 24 h of treatment (Fig. 6F and G). Moreover, nuclear flattening positively correlated with nuclear:cytoplasmic ratio of YAP and β-catenin (p < 0.001, Spearman's rank correlation) (Fig. 6H and I). Together, these results indicate that a viscous environment causes YAP and β-catenin activation through loss of cell-cell contacts and morphological changes.

3.7.   Viscosity-induced effects are substrate stiffness-dependent

The composition and mechanics of the ECM greatly affect cellular shape, phenotype and cancer malignancy [40-42]. Moreover, liver cancer cells grown on stiffer substrates, as found in liver fibrosis, present enhanced cell area, proliferation, and chemotherapeutic resistance in comparison with cells grown on soft healthy-liver-like substrates [40]. This led us to investigate whether there is a combined effect between substrate stiffness and fluid viscosity. By using elastic polyacrylamide gels functionalised with fibronectin (FN-PAA), we mimicked healthy (1 kPa) and fibrotic (10 kPa) livers. HepG2 cells on 1 kPa gels did not respond to high viscosity, but on 10 kPa and glass substrates, high viscosity enhanced cell area, cells appeared scattered instead of forming clusters, and contained nuclear β-catenin$^+$ and YAP$^+$ cells (Fig. 7A – D), although at a considerably lower percentage than cells grown on tissue culture polystyrene (Fig. 5D and E), probably due to differences in cell and nuclear morphology as a result of substrate stiffness and chemical composition. Similar effects were observed in PLC/PRF/5 cells, including the formation of large paxillin-containing focal adhesions, absent in HepG2 cells (Supplementary Fig. S6A – F). Also, traction force microscopy revealed significantly enhanced cellular traction forces on both cell types (Supplementary Fig. S6G and Fig. 7E and F). However, traction stresses (traction force per unit area) were only enhanced in viscous ECF-exposed HepG2 cells, which can be explained by the formation of stress fibres in this condition, but not in PLC/PRF/5 cells (Supplementary Fig. S6H and Fig. 6G). Thus,

indicating that the greater cellular traction force observed in PLC/PRF/5 cells is due to viscosity-induced larger spreading area. To elucidate whether the actin cytoskeleton contributes to viscosity-induced effects in cells adhered to compliant substrates, we pharmacologically disrupted the actin cytoskeleton in HepG2 cells seeded on a range of FN-PAA gels with increasing elastic moduli. This demonstrated an impact of cytoskeleton in ≤ 40 kPa substrates (Fig. 7H), inhibiting viscosity-induced cell area enhancement, cell scattering, and loss of YAP and β-catenin membrane localisation (Fig. 7I – K). These findings demonstrate the interplay between substrate mechanics and ECF viscosity in cell morphology, mechanotransduction, and traction force generation.

4. Discussion

Previous studies on macromolecular crowding using inert polymers have shown increased rates of biological reactions, including DNA ligase activity [20], antibody binding at the cell surface [43], and gene expression [44]. These effects are attributed to the volume exclusion that increases the effective concentrations of the molecules participating in the reaction. On the other hand, other biological reactions show lower rates upon macromolecular crowding [19, 45]. Here, we describe an effect of macromolecular crowding at the cellular level in which integrin-dependent cell adhesion is enhanced. However, macromolecular crowding alone does not explain the enhanced spreading rates as only large macromolecules such as 450,000 – 650,000 g mol^{-1} dextran or 1,000,000 g mol^{-1} PEG presented higher spreading rates than 20,000 g mol^{-1} PEG (Fig. S3 and Fig. 4D), but these *can* be attributed to differences in viscosity. The differing effects observed in macromolecules with different size have been defined as nano-viscosity [21]. Holyst R. *et al.* showed that the diffusion of proteins within macromolecule solutions experience low nano-viscosity when the diameter of the protein is smaller than the radius of gyration of the macromolecule [46]. However, the effect of nano-

viscosity using larger macromolecules, which could shed light on the identity of viscosity-sensing molecules, was not explored in this study.

Interestingly, viscosity not only affected cell spreading dynamics, but also induced enhanced migration, and the activation of intracellular signalling pathways leading to differential gene expression (Fig. 7L). In contrast to a previous study on fluid shear stress [35], we demonstrate that static viscous fluids without an active flow, as found in mucin-producing adenocarcinomas, can also induce cell migration (Fig. 1 and Fig. 2G). As previously reported [47, 48], cell scattering was abrogated by actin disruption and FAK inhibition (Fig. 3A and B), but actomyosin contractility induced protrusion formation and did not inhibit scattering (Fig. 3A and 3B and Supplementary Fig. S2I), effects that had been described in 2D cell cultures and might depend on the mode of migration of each cell type [49-51]. Conversely, these inhibitions did not affect cell area when these cells were adhered to very stiff tissue culture polystyrene (~ 1 GPa) (Fig. 3). Although the study presented here was performed in 2D cultures and may not be extrapolated to 3D and *in vivo*, we speculated a role for substrate stiffness in determining viscosity responsiveness. By using healthy liver-like (1 kPa) and fibrotic liver-like (10 kPa) substrates we mimicked more closely the *in vivo* environment of liver cancer cells. Strikingly, viscosity-enhanced cell area was abolished only in healthy liver-like conditions (Fig. 7A), similarly to previously observed responses to substrates of 1 kPa and 12 kPa in low viscosity conditions [40]. Moreover, in contrast to cells adhered to tissue culture polystyrene, at *in vivo*-like substrate stiffness, actin cytoskeleton disruption effectively inhibited viscosity-induced effects on cell area, cell scattering, and mechanotransduction pathway activation (Fig. 7H). These observations suggest there is a minimum force, determined by substrate stiffness and ECF viscosity, necessary to establish cellular adhesions to allow viscosity-induced cellular effects. These results are in line with previous reports on mechanosensing [25, 52] and were further confirmed by the enhanced traction forces observed in high viscosity conditions (Fig. S7G and Fig. 7F). However, the effect on total traction stresses was either less prominent in HepG2 cells or not significant in PLC/PRF/5 cells (Fig. S5H and Fig. 7G), which may indicate

that cells adapt to the mechanical load induced by enhanced viscosity by increasing their adhesion to the substrate leading to a larger cell area.

Cell area and geometry determine the state of intracellular cytoskeletal tension controlling the activation of mechanotransduction pathways and cell phenotype [53, 54]. Recent studies have demonstrated the role of the nucleus in the response to extracellular mechanical stimuli leading to transcription factor nuclear translocation and differential control of stem cell differentiation programs [39, 55]. Interestingly, HepG2 cells exposed to high ECF viscosity and adhered to tissue culture polystyrene presented nuclear flattening even after the pharmacological disruption of the actin cytoskeleton (Fig. 6F and G). This effect could be particularly relevant in cancer cells as these are inclined to present nuclear structural variations that can lead to softer nuclei, and thus, more easily deformable by external forces [56, 57]. Nuclear flattening correlated positively with YAP and β-catenin nuclear translocation, as previously described in a different cell type [39]. However, the nuclear translocation of YAP and β-catenin only elicited an enhanced AREG gene expression, a gene encoding for amphiregulin, which has been involved in cancer cell migration, but other known targets of YAP and β-catenin were either unchanged or downregulated (Fig. 5B and C). The downregulated genes BIRC5 and CTGF have both been linked to EMT [37, 38], which could be related to the downregulation of mesenchymal genes observed (Fig. 2I and J). These results suggest that the observed mesenchymal behaviour cannot be explained by a differential gene expression but is due to a direct effect on the cellular machinery controlling cell migration. This may also explain the different behaviour observed within epithelial cell lines (Fig. 1B), suggesting that the expression of viscosity-sensing or viscosity-responding proteins that allow cell migration will determine the responsiveness to high viscosity. Understanding the process and the identification of the molecular players involved in viscosity sensing will allow the prediction of responsiveness to high viscosity in different cell types.

In summary, here we report a previously undescribed effect, to our knowledge, of static ECF viscosity on cell behaviour. High viscosity facilitates cell-substrate integrin-based adhesions,

leading to enhanced cell migration and loss of cluster cohesiveness. Interestingly, these effects are observed in both inert polymer- and mucin-containing ECF. Also, the ECM stiffening occurring in the cancer microenvironment [41] is necessary for the viscosity-related effects described here. On the other hand, ECF viscosity alters the response of cells to their substrate. This suggests that an enhanced microenvironmental viscosity may exacerbate the response to enhanced ECM stiffness, which has been used to improve biomaterial design to alter cell behaviour. Finally, ECF viscosity-enhancing molecules may constitute a potential therapeutic target for cancer, when reducing ECM stiffness is not feasible.

Author contributions:

J.G.-M. conceived the study, designed the experiments and prepared the manuscript. J.G.-M and X.Z. performed traction force experiments. X.Z. performed live imaging studies. X.Z. and N.G. analysed traction force and live imaging experiments. J.G.-M., M.B. and M.A. carried out and analysed fluorescence and confocal imaging experiments. J.G.-M. and J.M.S. performed wound healing and cell scattering experiments. B.F. and C.S. were involved in experimental design. All authors discussed results and participated in the development of the manuscript.

References

[1] J.D. Humphrey, E.R. Dufresne, M.A. Schwartz, Mechanotransduction and extracellular matrix homeostasis, Nature reviews. Molecular cell biology 15(12) (2014) 802-12.

[2] L. Li, J. Eyckmans, C.S. Chen, Designer biomaterials for mechanobiology, Nature materials 16(12) (2017) 1164-1168.

[3] D.E. Jaalouk, J. Lammerding, Mechanotransduction gone awry, Nat Rev Mol Cell Bio 10(1) (2009) 63-73.

[4] C.H. Heldin, K. Rubin, K. Pietras, A. Ostman, High interstitial fluid pressure - an obstacle in cancer therapy, Nature reviews. Cancer 4(10) (2004) 806-13.

[5] A.J. Kosmalska, L. Casares, A. Elosegui-Artola, J.J. Thottacherry, R. Moreno-Vicente, V. Gonzalez-Tarrago, M.A. del Pozo, S. Mayor, M. Arroyo, D. Navajas, X. Trepat, N.C. Gauthier, P. Roca-Cusachs, Physical principles of membrane remodelling during cell mechanoadaptation, Nat Commun 6 (2015) 7292.

[6] C. Voutouri, T. Stylianopoulos, Evolution of osmotic pressure in solid tumors, Journal of biomechanics 47(14) (2014) 3441-7.

[7] A.S. Piotrowski-Daspit, J. Tien, C.M. Nelson, Interstitial fluid pressure regulates collective invasion in engineered human breast tumors via Snail, vimentin, and E-cadherin, Integrative biology : quantitative biosciences from nano to macro 8(3) (2016) 319-31.

[8] M. Hofmann, M. Guschel, A. Bernd, J. Bereiter-Hahn, R. Kaufmann, C. Tandi, H. Wiig, S. Kippenberger, Lowering of tumor interstitial fluid pressure reduces tumor cell proliferation in a xenograft tumor model, Neoplasia 8(2) (2006) 89-95.

[9] Y.N. Andrade, J. Fernandes, E. Vazquez, J.M. Fernandez-Fernandez, M. Arniges, T.M. Sanchez, M. Villalon, M.A. Valverde, TRPV4 channel is involved in the coupling of fluid viscosity changes to epithelial ciliary activity, J Cell Biol 168(6) (2005) 869-874.

[10] B.J. Ballermann, A. Dardik, E. Eng, A.L. Liu, Shear stress and the endothelium, Kidney Int 54 (1998) S100-S108.

[11] S.S. Ranade, Z.Z. Qiu, S.H. Woo, S.S. Hur, S.E. Murthy, S.M. Cahalan, J. Xu, J. Mathur, M. Bandell, B. Coste, Y.S.J. Li, S. Chien, A. Patapoutian, Piezo1, a mechanically activated ion channel, is required for vascular development in mice, P Natl Acad Sci USA 111(28) (2014) 10347-10352.

[12] J. Li, B. Hou, S. Tumova, K. Muraki, A. Bruns, M.J. Ludlow, A. Sedo, A.J. Hyman, L. McKeown, R.S. Young, N.Y. Yuldasheva, Y. Majeed, L.A. Wilson, B. Rode, M.A. Bailey, H.R. Kim, Z.J. Fu, D.A.L. Carter, J. Bilton, H. Imrie, P. Ajuh, T.N. Dear, R.M. Cubbon, M.T. Kearney, K.R. Prasad, P.C. Evans, J.F.X. Ainscough, D.J. Beech, Piezo1 Integration of Vascular Architecture with Physiological Force, Faseb J 29 (2015).

[13] H.J. Lee, M.F. Diaz, K.M. Price, J.A. Ozuna, S.L. Zhang, E.M. Sevick-Muraca, J.P. Hagan, P.L. Wenzel, Fluid shear stress activates YAP1 to promote cancer cell motility, Nat Commun 8 (2017).

[14] N.K. Lee, S. Kim, H.S. Kim, T.Y. Jeon, G.H. Kim, D.U. Kim, D.Y. Park, T.U. Kim, D.H. Kang, Spectrum of mucin-producing neoplastic conditions of the abdomen and pelvis: cross-sectional imaging evaluation, World J Gastroenterol 17(43) (2011) 4757-71.

[15] R.J. Roselli, K.R. Diller, SpringerLink, Biotransport: Principles and Applications, Springer New York : Imprint: Springer, New York, NY, 2011.

[16] D.W. Kufe, Mucins in cancer: function, prognosis and therapy, Nature Reviews Cancer 9(12) (2009) 874-885.

[17] R.E. Wells, Jr., E.W. Merrill, Shear rate dependence of the viscosity of whole bllod and plasma, Science 133(3455) (1961) 763-4.

[18] R.J. Ellis, Macromolecular crowding: obvious but underappreciated, Trends Biochem Sci 26(10) (2001) 597-604.

[19] C.P. Papaneophytou, A.I. Grigoroudis, C. McInnes, G. Kontopidis, Quantification of the Effects of Ionic Strength, Viscosity, and Hydrophobicity on Protein-Ligand Binding Affinity, Acs Med Chem Lett 5(8) (2014) 931-936.

[20] S.B. Zimmerman, B.H. Pheiffer, Macromolecular Crowding Allows Blunt-End Ligation by DNA Ligases from Rat-Liver or Escherichia-Coli, P Natl Acad Sci-Biol 80(19) (1983) 5852-5856.

[21] S. Hou, N. Ziebacz, T. Kalwarczyk, T.S. Kaminski, S.A. Wieczorek, R. Holyst, Influence of nano-viscosity and depletion interactions on cleavage of DNA by enzymes in glycerol and poly(ethylene glycol) solutions: qualitative analysis, Soft Matter 7(7) (2011) 3092-3099.

[22] J.D. Humphrey, E.R. Dufresne, M.A. Schwartz, Mechanotransduction and extracellular matrix homeostasis, Nat Rev Mol Cell Bio 15(12) (2014) 802-812.

[23] V. Swaminathan, C.M. Waterman, The molecular clutch model for mechanotransduction evolves, Nat Cell Biol 18(5) (2016) 459-461.

[24] A. Elosegui-Artola, R. Oria, Y.F. Chen, A. Kosmalska, C. Perez-Gonzalez, N. Castro, C. Zhu, X. Trepat, P. Roca-Cusachs, Mechanical regulation of a molecular clutch defines force transmission and transduction in response to matrix rigidity, Nat Cell Biol 18(5) (2016) 540-+.

[25] M. Bennett, M. Cantini, J. Reboud, J.M. Cooper, P. Roca-Cusachs, M. Salmeron-Sanchez, Molecular clutch drives cell response to surface viscosity, Proc Natl Acad Sci U S A (2018).

[26] S.V. Plotnikov, A.M. Pasapera, B. Sabass, C.M. Waterman, Force Fluctuations within Focal Adhesions Mediate ECM-Rigidity Sensing to Guide Directed Cell Migration, Cell 151(7) (2012) 1513-1527.

[27] T. Geback, M.M. Schulz, P. Koumoutsakos, M. Detmar, TScratch: a novel and simple software tool for automated analysis of monolayer wound healing assays, BioTechniques 46(4) (2009) 265-74.

[28] Y. Aratyn-Schaus, P.W. Oakes, J. Stricker, S.P. Winter, M.L. Gardel, Preparation of complaint matrices for quantifying cellular contraction, Journal of visualized experiments : JoVE (46) (2010).

[29] J.R. Tse, A.J. Engler, Preparation of hydrogel substrates with tunable mechanical properties, Current protocols in cell biology Chapter 10 (2010) Unit 10 16.

[30] M. Yilmaz, G. Christofori, EMT, the cytoskeleton, and cancer cell invasion, Cancer Metast Rev 28(1-2) (2009) 15-33.

[31] D.D. Shao, W. Xue, E.B. Krall, A. Bhutkar, F. Piccioni, X.X. Wang, A.C. Schinzel, S. Sood, J. Rosenbluh, J.W. Kim, Y. Zwang, T.M. Roberts, D.E. Root, T. Jacks, W.C. Hahn, KRAS and YAP1 Converge to Regulate EMT and Tumor Survival, Cell 158(1) (2014) 171-184.

[32] B.W. Benham-Pyle, B.L. Pruitt, W.J. Nelson, Mechanical strain induces E-cadherin-dependent Yap1 and beta-catenin activation to drive cell cycle entry, Science 348(6238) (2015) 1024-1027.

[33] S. Dupont, L. Morsut, M. Aragona, E. Enzo, S. Giulitti, M. Cordenonsi, F. Zanconato, J. Le Digabel, M. Forcato, S. Bicciato, N. Elvassore, S. Piccolo, Role of YAP/TAZ in mechanotransduction, Nature 474(7350) (2011) 179-U212.

[34] S.C. Wei, L. Fattet, J.H. Tsai, Y.R. Guo, V.H. Pai, H.E. Majeski, A.C. Chen, R.L. Sah, S.S. Taylor, A.J. Engler, J. Yang, Matrix stiffness drives epithelial mesenchymal transition and tumour metastasis through a TWIST1-G3BP2 mechanotransduction pathway, Nat Cell Biol 17(5) (2015) 678-U306.

[35] H.J. Lee, M.F. Diaz, K.M. Price, J.A. Ozuna, S. Zhang, E.M. Sevick-Muraca, J.P. Hagan, P.L. Wenzel, Fluid shear stress activates YAP1 to promote cancer cell motility, Nat Commun 8 (2017) 14122.

[36] J. Zhang, J.Y. Ji, M. Yu, M. Overholtzer, G.A. Smolen, R. Wang, J.S. Brugge, N.J. Dyson, D.A. Haber, YAP-dependent induction of amphiregulin identifies a non-cell-autonomous component of the Hippo pathway, Nat Cell Biol 11(12) (2009) 1444-50.

[37] S. Sonnylal, S. Xu, H. Jones, A. Tam, V.R. Sreeram, M. Ponticos, J. Norman, P. Agrawal, D. Abraham, B. de Crombrugghe, Connective tissue growth factor causes EMT-like cell fate changes in vivo and in vitro, J Cell Sci 126(Pt 10) (2013) 2164-75.

[38] C.J. Tai, C.S. Hung, L.J. Kuo, P.L. Wei, H.H. Lu, H.A. Chen, T.Z. Liu, J.J. Liu, D.Z. Liu, Y.S. Ho, C.H. Wu, Y.J. Chang, Survivin-Mediated Cancer Cell Migration Through GRP78

and Epithelial-Mesenchymal Transition (EMT) Marker Expression in Mahlavu Cells, Ann Surg Oncol 19(1) (2012) 336-343.

[39] A. Elosegui-Artola, I. Andreu, A.E.M. Beedle, A. Lezamiz, M. Uroz, A.J. Kosmalska, R. Oria, J.Z. Kechagia, P. Rico-Lastres, A.L. Le Roux, C.M. Shanahan, X. Trepat, D. Navajas, S. Garcia-Manyes, P. Roca-Cusachs, Force Triggers YAP Nuclear Entry by Regulating Transport across Nuclear Pores, Cell 171(6) (2017) 1397-1410 e14.

[40] J. Schrader, T.T. Gordon-Walker, R.L. Aucott, M. van Deemter, A. Quaas, S. Walsh, D. Benten, S.J. Forbes, R.G. Wells, J.P. Iredale, Matrix Stiffness Modulates Proliferation, Chemotherapeutic Response, and Dormancy in Hepatocellular Carcinoma Cells, Hepatology 53(4) (2011) 1192-1205.

[41] P.F. Lu, V.M. Weaver, Z. Werb, The extracellular matrix: A dynamic niche in cancer progression, J Cell Biol 196(4) (2012) 395-406.

[42] A. Engler, L. Bacakova, C. Newman, A. Hategan, M. Griffin, D. Discher, Substrate compliance versus ligand density in cell on gel responses, Biophysical journal 86(1 Pt 1) (2004) 617-28.

[43] R. Chapanian, D.H. Kwan, I. Constantinescu, F.A. Shaikh, N.A.A. Rossi, S.G. Withers, J.N. Kizhakkedathu, Enhancement of biological reactions on cell surfaces via macromolecular crowding, Nat Commun 5 (2014).

[44] C.M. Tan, S. Saurabh, M.P. Bruchez, R. Schwartz, P. LeDuc, Molecular crowding shapes gene expression in synthetic cellular nanosystems, Nat Nanotechnol 8(8) (2013) 602-608.

[45] S. Hou, P. Trochimczyk, L.L. Sun, A. Wisniewska, T. Kalwarczyk, X.Z. Zhang, B. Wielgus-Kutrowska, A. Bzowska, R. Holyst, How can macromolecular crowding inhibit biological reactions? The enhanced formation of DNA nanoparticles, Sci Rep-Uk 6 (2016).

[46] R. Holyst, A. Bielejewska, J. Szymanski, A. Wilk, A. Patkowski, J. Gapinski, A. Zywocinski, T. Kalwarczyk, E. Kalwarczyk, M. Tabaka, N. Ziebacz, S.A. Wieczorek, Scaling form of viscosity at all length-scales in poly(ethylene glycol) solutions studied by fluorescence correlation spectroscopy and capillary electrophoresis, Phys Chem Chem Phys 11(40) (2009) 9025-9032.

[47] J.F. Lai, S.C. Kao, S.T. Jiang, M.J. Tang, P.C. Chan, H.C. Chen, Involvement of focal adhesion kinase in hepatocyte growth factor-induced scatter of Madin-Darby canine kidney cells, J Biol Chem 275(11) (2000) 7474-7480.

[48] H. Yamaguchi, J. Condeelis, Regulation of the actin cytoskeleton in cancer cell migration and invasion, Bba-Mol Cell Res 1773(5) (2007) 642-652.

[49] W.C. Hung, S.H. Chen, C.D. Paul, K.M. Stroka, Y.C. Lo, J.T. Yang, K. Konstantopoulos, Distinct signaling mechanisms regulate migration in unconfined versus confined spaces, J Cell Biol 202(5) (2013) 807-24.

[50] R.J. Petrie, N. Gavara, R.S. Chadwick, K.M. Yamada, Nonpolarized signaling reveals two distinct modes of 3D cell migration, J Cell Biol 197(3) (2012) 439-55.

[51] A.I. Ivanov, A.M. Hopkins, G.T. Brown, K. Gerner-Smidt, B.A. Babbin, C.A. Parkos, A. Nusrat, Myosin II regulates the shape of three-dimensional intestinal epithelial cysts, J Cell Sci 121(11) (2008) 1803-14.

[52] L. Jiang, Z.L. Sun, X.F. Chen, J. Li, Y. Xu, Y. Zu, J.L. Hu, D. Han, C. Yang, Cells Sensing Mechanical Cues: Stiffness Influences the Lifetime of Cell-Extracellular Matrix Interactions by Affecting the Loading Rate, Acs Nano 10(1) (2016) 207-217.

[53] K.A. Kilian, B. Bugarija, B.T. Lahn, M. Mrksich, Geometric cues for directing the differentiation of mesenchymal stem cells, Proc Natl Acad Sci U S A 107(11) (2010) 4872-7.

[54] S. Dupont, L. Morsut, M. Aragona, E. Enzo, S. Giulitti, M. Cordenonsi, F. Zanconato, J. Le Digabel, M. Forcato, S. Bicciato, N. Elvassore, S. Piccolo, Role of YAP/TAZ in mechanotransduction, Nature 474(7350) (2011) 179-83.

[55] J. Swift, I.L. Ivanovska, A. Buxboim, T. Harada, P.C. Dingal, J. Pinter, J.D. Pajerowski, K.R. Spinler, J.W. Shin, M. Tewari, F. Rehfeldt, D.W. Speicher, D.E. Discher, Nuclear lamin-A scales with tissue stiffness and enhances matrix-directed differentiation, Science 341(6149) (2013) 1240104.

[56] D. Zink, A.H. Fischer, J.A. Nickerson, Nuclear structure in cancer cells, Nature reviews. Cancer 4(9) (2004) 677-87.
[57] C. Denais, J. Lammerding, Nuclear mechanics in cancer, Advances in experimental medicine and biology 773 (2014) 435-70.
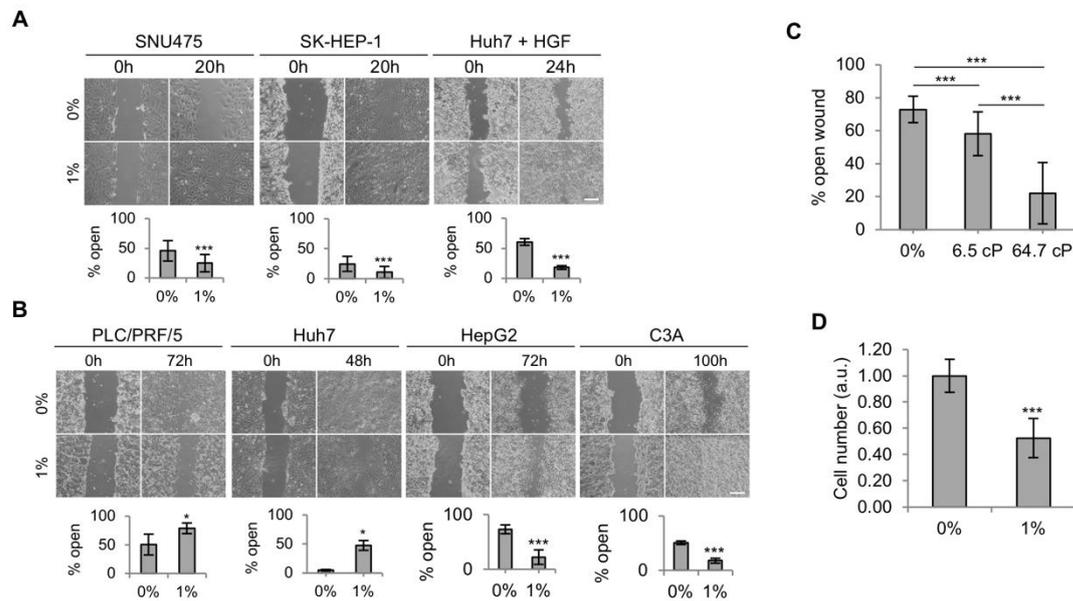
Figures

Fig. 1. Soluble sodium alginate affects wound healing in epithelial and mesenchymal liver cell lines differently. **A**, Cell lines with mesenchymal phenotype show significantly improved wound healing in 1% Na-alginate-containing medium (n = 3). Scale bar, 200 μm. **B**, Epithelial cell lines present both significantly reduced (PLC/PRF/5 and Huh7) and enhanced (HepG2 and C3A) wound healing upon 1% Na-alginate exposure (n = 3). Scale bar, 200 μm. **C**, Wound healing is significantly enhanced after 72 h exposure to 64.7 cP 1% Na-alginate compared to 6.5 cP 1% Na-alginate (n = 4). **D**, Quantification of HepG2 cell nuclei after 4 days culture indicates reduced cell number in 1% Na-alginate compared with 0% control (n = 5). Data represents average ± s.e.m. (**A-C**) or average ± s.d. (**D**). Statistical significance was assessed by two-tailed Student's *t*-test (**A**, **B**, **D**) or one-way ANOVA with Tukey's multiple comparison test (**C**). * $p < 0.05$; *** $p < 0.001$.
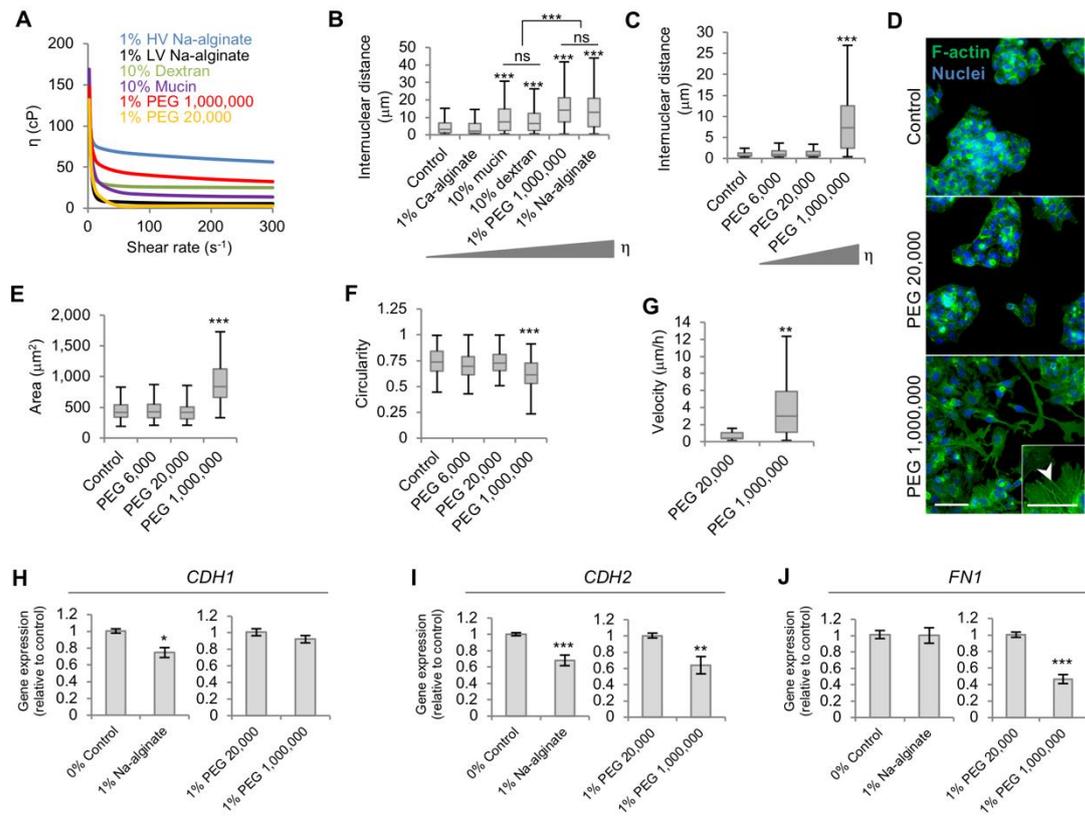
Fig. 2. Extracellular viscosity causes cell scattering and morphological changes without a mesenchymal gene expression switch. A, Average viscosities (η) of viscosity enhancers at 1% (w/v) for Na-alginate and PEG and 10% (w/v) for dextran and mucin (n = 3). **B**, Internuclear distance of HepG2 cell clusters increases after 24 h exposure to viscosity enhancers causing cell scattering (n = 300 nuclei). **C**, Internuclear distance is enhanced in HepG2 cells incubated for 24 h with 1% PEG 1,000,000 (highest η) but not low molecular weight PEG (n = 600 nuclei). **D**, A 24 h exposure to 1% PEG 1,000,000 causes loss of cell-cell junctions, formation of lamellipodia and stress fibres (arrowhead) in HepG2 cells. Scale bars: 50 μm (larger images) and 25 μm (inset). **E**, **F**, Cells from (**D**) present a larger cell area (**E**) and reduced circularity (**F**) when treated with PEG 1,000,000 (n = 250 cells). All boxplots represent: median, first and third quartiles; whiskers indicate maximum and minimum within 1.5x the interquartile range. **G**, Single HepG2 cells have higher velocity in viscous

environments (n = 29 cells for PEG 20,000 and n = 40 cells for PEG 1,000,000). **H** − **J**, Quantification of gene expression relative to low viscosity controls (0% or 1% PEG 1,000,000) of *CDH1* (**H**), *CDH2* (**I**), and *FN1* (**J**) in cells cultured for 2 days (n = 3). Bar graphs indicate average ± s.e.m and boxplots represent the median, first and third quartiles; whiskers indicate maximum and minimum within 1.5x the interquartile range. Statistical significance was assessed by One-way ANOVA with Tukey's test (**B**, **C**, **E**) or two-tailed Student's *t*-test (**D**, **F**-**H**). ns $p > 0.05$; * $p < 0.05$; ** $p < 0.01$; *** $p < 0.001$.
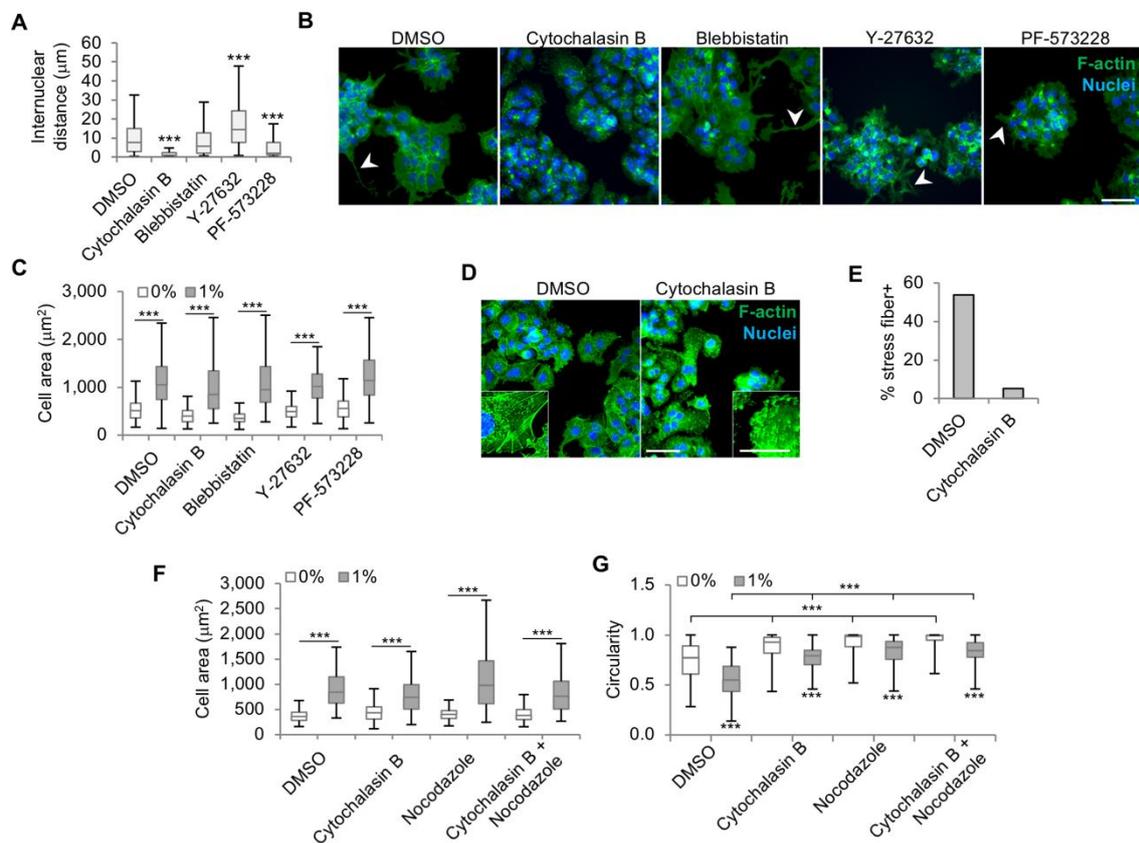

Fig. 3. Viscosity-enhanced cell size is independent of actin cytoskeleton and microtubule integrity. A, Quantification of internuclear distance in HepG2 cell clusters in 1% Na-alginate shows dependence on actin cytoskeleton integrity and FAK but not on actomyosin contractility in viscosity-induced cell scattering (n = 600 nuclei). **B**, Fluorescent images of

HepG2 cell clusters treated for 12 h with 1% Na-alginate and the indicated molecules used in (**A**). Arrowheads show formation of cellular protrusions. Scale bar, 50 μm. **C**, Viscosity-enhanced cell area in HepG2 cells is independent of actomyosin and FAK (n = 150 cells). **D**, Fluorescent images of HepG2 cells in 1% Na-alginate treated with DMSO (control) or cytochalasin B demonstrating efficient disruption of actin fibres. Scale bar, 50 μm for large images and 20 μm for insets. **E**, Quantification of stress-fibre-presenting cells from (**D**) (n > 600 cells). **F**, Quantification of HepG2 cell area in cells treated with 0% or 1% Na-alginate and the indicated inhibitors or control (DMSO) for 24 h shows no abrogation of viscosity-enhanced cell area (n > 150 cells). **G**, Circularity of cells from (**F**) is enhanced upon F-actin and microtubule inhibition (n > 150 cells per condition). All boxplots represent the median, first and third quartiles; whiskers indicate maximum and minimum within 1.5x the interquartile range. Statistical analyses: One-way ANOVA with Tukey's multiple comparison test. *** $p < 0.001$.
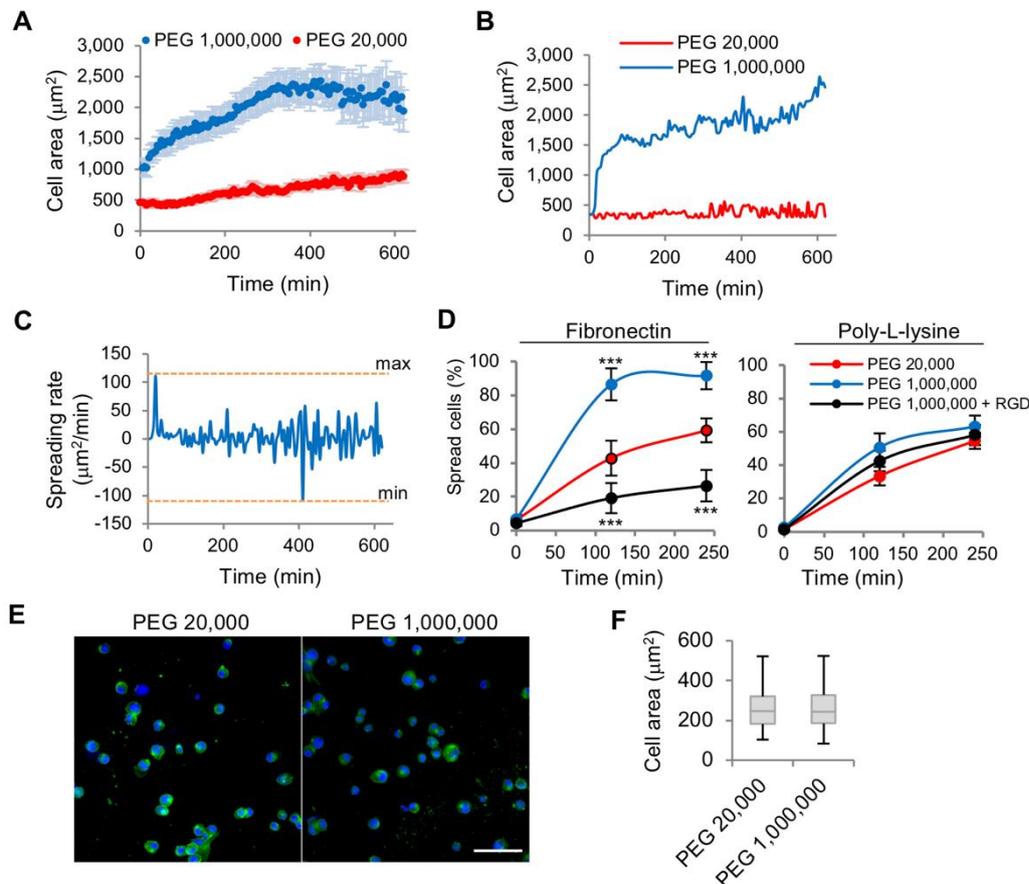
Fig. 4. Viscosity causes an integrin-dependent cell spreading. **A**, Average cell area of single HepG2 cells over time. Data points indicate average ± s.e.m (n = 9 cells for PEG 20,000 and n = 11 cells for PEG 1,000,000). **B**, Examples of individual cells from (**A**). **C**, Cell spreading rate of a single cell exposed to PEG 1,000,000 from (**B**). **D**, Quantification of spread HepG2 cells attached to fibronectin-glass or poly-L-lysine-glass (PLL-glass) over time shows faster cell spreading in viscous media, effect dependent on integrin adhesion. Data points indicate average ± s.e.m (n = 4, > 100 cells per condition per repeat). **E**, **F**, A 4 h culture in high ECF viscosity does not affect cell morphology of cells adhered to PLL-glass. Scale bar: 50 μm. All boxplots represent: median, first and third quartiles; whiskers indicate maximum and minimum within 1.5x the interquartile range. Statistical significance was assessed by ANOVA with Tukey's test (**D**) or two-tailed Student's t-test (**F**). *** $p < 0.001$.
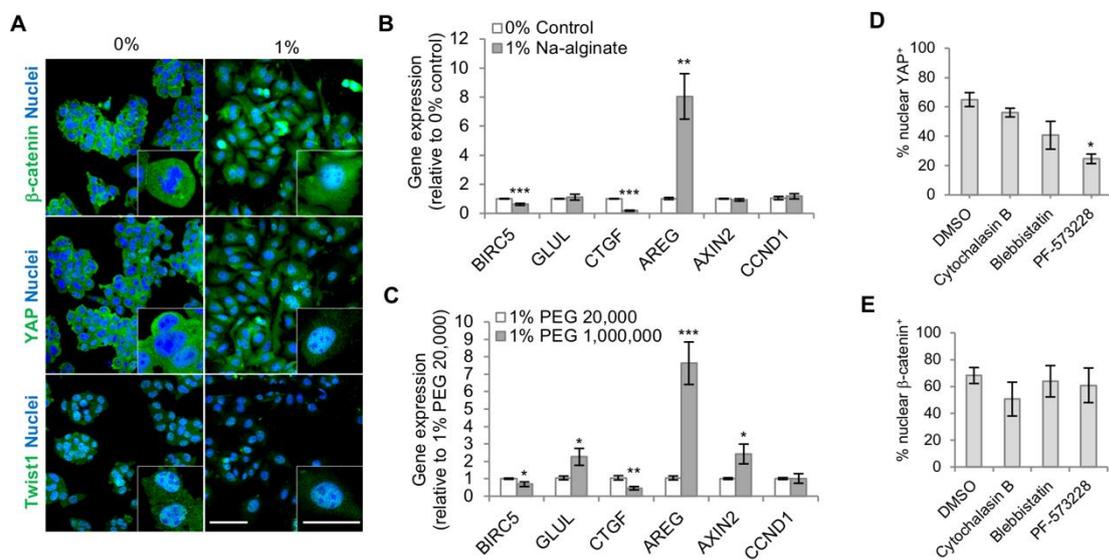

Fig. 5. High viscosity causes YAP and β-catenin nuclear translocation. **A**, HepG2 cells treated with 0% or 1% Na-alginate for 24 h present differences in subcellular localisation of YAP and β-catenin but not Twist1. Scale bar, 50 μm (25 μm insets). **B**, **C**, Quantification of gene expression of survivin (*BIRC5*), glutamine synthetase (*GLUL*), connective tissue growth

factor (*CTGF*), cyclin D1 (*CCND1*), amphiregulin (*AREG*), and axin-2 (*AXIN2*) normalised to controls (0% control (**B**) or 1% PEG 20,000 (**C**)) of cells cultured for 2 days with the indicated polymer-containing media (n = 3). **D**, **E**, Percentage of nuclear YAP[+] (**D**) and β-catenin[+] (**E**) HepG2 cells (nuclear:cytoplasmic fluorescence intensity ratio > 1.5) in 1% Na-alginate for 24 h are unaffected by actomyosin inhibition or FAK inhibition (**E**) (n = 3). All data represent the average ± s.e.m. Statistical analyses: two-tailed Student's t-test (**B**, **C**) ore one-way ANOVA with Tukey's multiple comparison test (**D**, **E**). * $p < 0.05$; ** $p < 0.01$; *** $p < 0.001$.
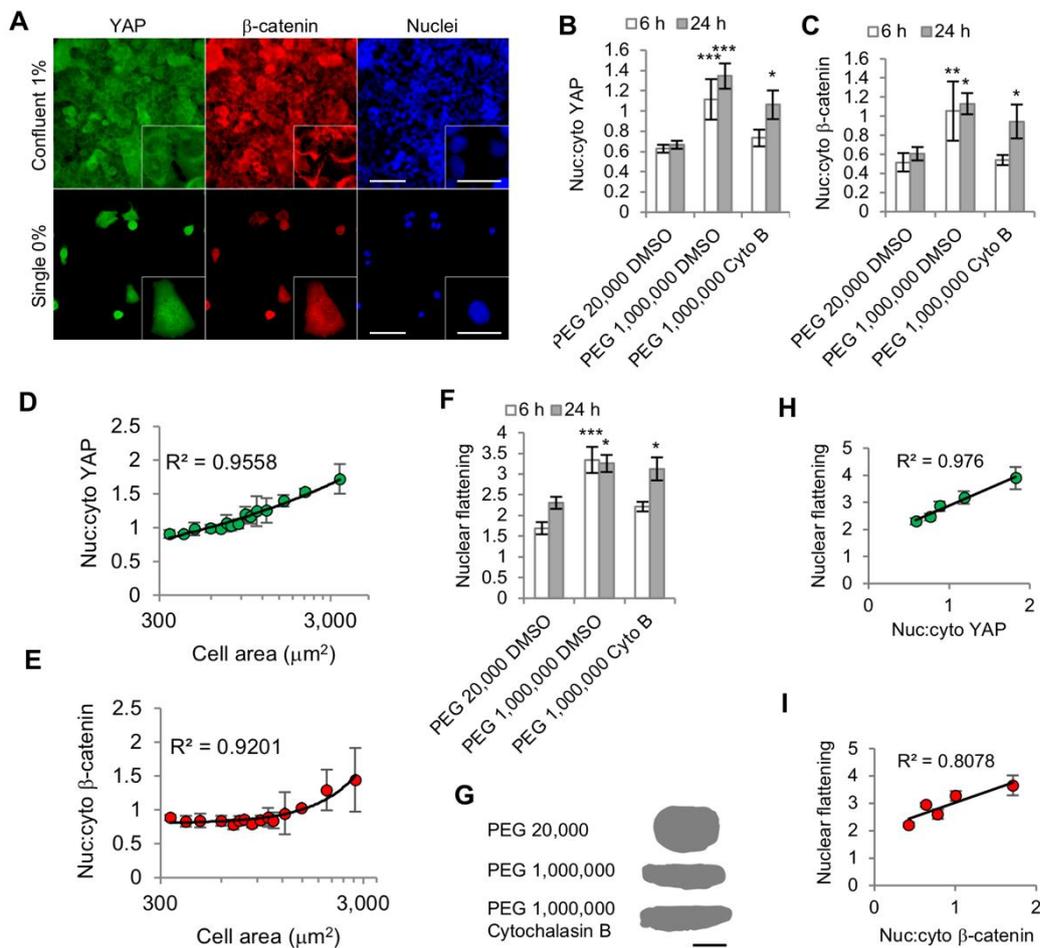

Fig. 6. Cell morphology and cell-cell contacts regulate YAP and b-catenin localisation.

A, Cell crowding blocks YAP and β-catenin nuclear translocation induced by 1% Na-alginate.

Scale bars, 50 μm (20 μm insets). **B**, **C**, Nuclear:cytoplasmic ratio of YAP (**B**) and β-catenin (**C**) in single cells from confocal fluorescence intensities is after 6 h or 24 h (n ≥ 10 cells per condition). **D**, **E**, Correlation between fluorescence intensity of nuclear:cytoplasmic YAP ratio (**D**) and nuclear:cytoplasmic b-catenin ratio (**E**) and cell area in single HepG2 cells (R^2, squared correlation coefficient; n ≥ 150 cells). **F**, Nuclear flattening (length/height) of cells from (**B**) and (**C**). **G**, Example lateral views of nuclei from (**F**). Scale bar, 10 μm. **H**, **I**, Nuclear flattening versus nuclear:cytoplasmic ratio of YAP (**H**) or β-catenin (**I**) of cells from (**B**, **C**, and **F**) indicating a positive correlation (R^2, squared correlation coefficient; n = 35 cells). All bar graphs represent the average ± s.e.m. Statistical analyses: Kruskal-Wallis test with Dunn's multiple comparison test. *ns* p > 0.05; * p < 0.05; *** p < 0.001.

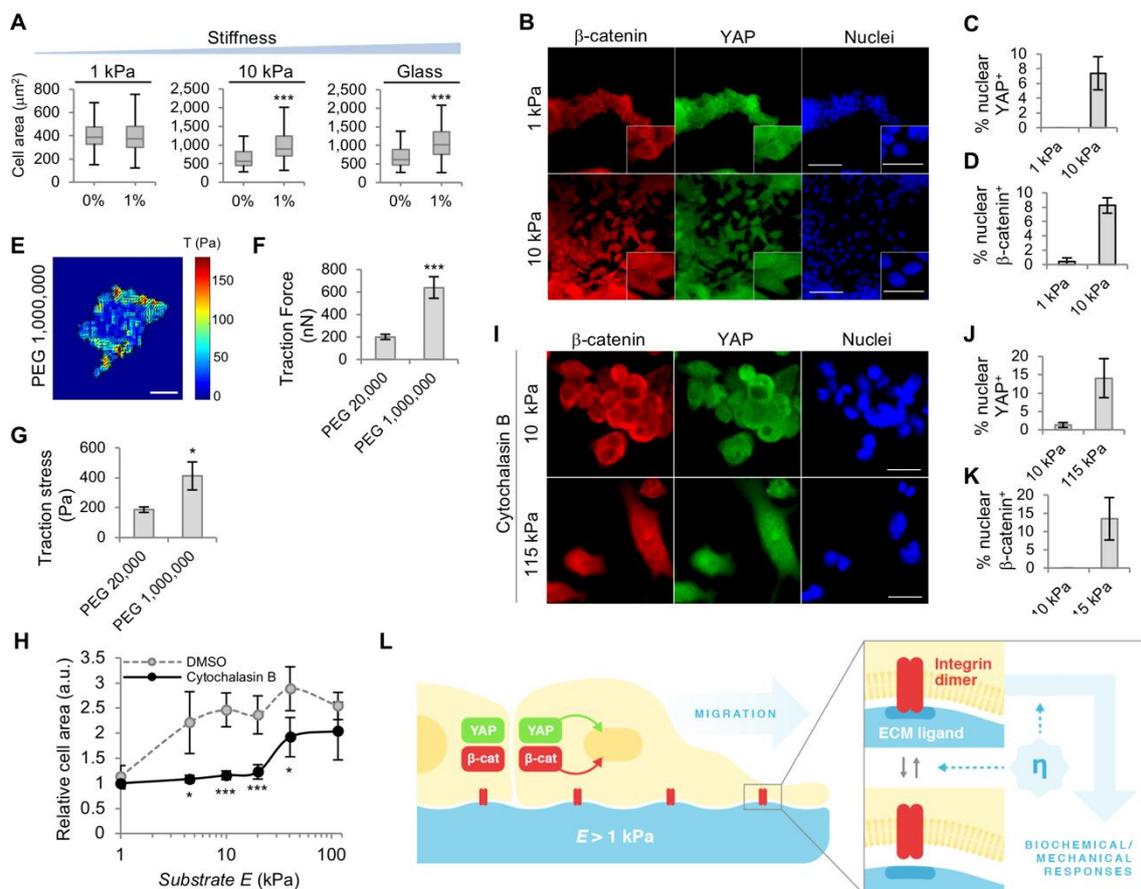**Fig. 7. Cell morphology and cell-cell contacts regulate YAP and β-catenin localisation**.

A, Cell crowding blocks YAP and β-catenin nuclear translocation induced by 1% Na-alginate. Scale bars, 50 μm (20 μm insets). **B**, **C**, Nuclear:cytoplasmic ratio of YAP (**B**) and β-catenin (**C**) in single cells from confocal fluorescence intensities is enhanced in 1% PEG 1,000,000 after 24 h (n ≥ 10 cells per condition). **D**, **E**, Correlation between fluorescence intensity of nuclear:cytoplasmic YAP ratio (**D**) and nuclear:cytoplasmic β-catenin ratio (**E**) and cell area in single HepG2 cells (R^2, squared correlation coefficient; n ≥ 150 cells). **F**, Nuclear flattening (length/height) of cells from (**B**) and (**D**). **G**, Example lateral views of nuclei from (**F**). Scale bar, 10 μm. **H**, **I**, Nuclear flattening versus nuclear:cytoplasmic ratio of YAP (**H**) or β-catenin (**I**) of cells from (**B**, **C**, **F**) indicating a positive correlation (R^2, squared correlation coefficient; n = 35 cells). Data points indicate average± s.e.m. All bar graphs represent the average ± s.e.m. Statistical analyses: Kruskal-Wallis test with Dunn's multiple comparison test. *ns* p > 0.05; * p < 0.05; *** p < 0.001.